

LignoPhot: Photoactive hybrid lignin/Bi₄O₅Br₂/BiOBr composite for complex pollutants removal

Tetyana M. Budnyak[§], Joy Onwumere[§], Ievgen V. Pylypchuk, Aleksander Jaworski, Jianhong Chen, Anna Rokicińska, Mikael E. Lindström, Piotr Kuśtrowski, Olena Sevastyanova, and Adam Slabon*

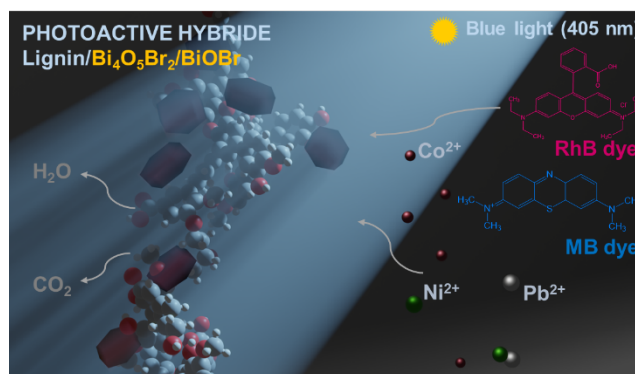
ABSTRACT: Valorization of lignin is still an open question and lignin has therefore remained an underutilized biomaterial. This situation is even more pronounced for hydrolysis lignin, which is characterized by a highly condensed and excessively cross-linked structure. We report on photoactive lignin/Bi₄O₅Br₂/BiOBr bio-inorganic composites consisting of a lignin substrate that is coated by Bi₄O₅Br₂/BiOBr nanosheet photocatalysts. The structure of the hybrid material was investigated by means of X-ray diffraction (XRD), X-ray photoelectron spectroscopy (XPS), scanning electron microscopy (SEM), transmission electron microscopy including energy dispersive X-ray (EDX) spectroscopy, and solid state ¹H-¹³C nuclear magnetic resonance spectroscopy (¹H-¹³C NMR). The material contains 18.9% of Bi₄O₅Br₂/BiOBr and was found to be effective for the photocatalytic degradation of cationic methylene blue (MB) and zwitterionic rhodamine B (RhB) dyes under irradiation with 405 nm light. Lignin/Bi₄O₅Br₂/BiOBr was able to decrease the dye concentration from 80 mg·L⁻¹ to 12.3 mg·L⁻¹ for RhB (85%) and from 80 mg·L⁻¹ to 4.4 mg·L⁻¹ for MB (95%). Complementary to the dye degradation, the lignin as a main component of the composite, was found to be efficient and rapid biosorbent for metal ions in aqueous solutions. The highest adsorption capacity was found after 2 hours of phases contact and reached 0.45 mmol·g⁻¹ for Ni(II) ions (neutral media). The low cost, simplicity of the synthesis, good stability and ability to simultaneously photooxidize organic dyes and to adsorb metal ions, make the developed photoactive lignin/Bi₄O₅Br₂/BiOBr composite a prospective material for textile wastewaters remediation.

Keywords: photocatalysis, hydrolysis lignin, bioinorganic interfaces, adsorption, water treatment

INTRODUCTION

The transition to a circular economy has to be accelerated for achieving the environmental and climate objectives and Global Goals in the 2030 Agenda. The sustainable utilization of resources increases their lifespan and value, and decrease the need for the extraction of new raw materials and landfill waste.¹ For example, more than 0.7 million tons of synthetic dyes are produced annually for using in textile, leather, cosmetics, paper, paint, and food industries.² In the textile industry more than 10,000 different dyes and pigments are being used continuously, leading to a variety of organic and inorganic pollutants being discharged on each step of textile production.^{3,4} Precipitation, coagulation, oxidation and adsorption have been applied for the treatment of wastewaters containing dyes; however, all those methods have specific disadvantages: high cost, lack of complete removal of dyes from wastewater, limited removal efficiency, low selectivity and additional waste production. Therefore, there is an urgent need for development of materials that combine multifunctionality for simultaneous and sustainable removal of different classes of toxicants.⁵ Certain semiconductor nanostructures can harvest light and achieve efficient charge carrier separation to drive subsequent photochemical processes.⁶⁻¹¹

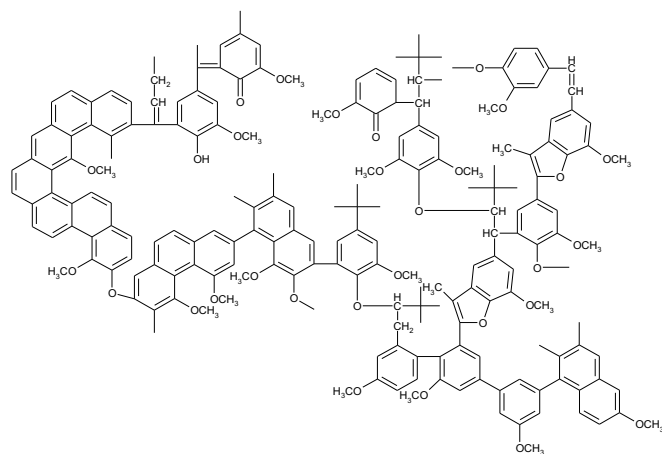
From an environmental and scientific point of view, there is a critical demand for materials prepared from renewable bio-sources.¹²⁻¹⁷ We recently presented the *Celluphot* concept that encompasses a hydrothermally grown two-dimensional photocatalyst on a mechanically stable cellulose membrane.¹⁸ This



bio-inorganic material exhibits dual functionality, i.e. photocatalysis and adsorption of metal ions. An important aspect is the low synthesis temperature of 115 °C for the semiconducting heterojunction Bi₄O₅Br₂/BiOBr nanosheets, because this allows to maintain the functional groups of the biobased substrate. A similar approach can be also utilized to grow TiO₂ nanorods on cellulosic substrates.¹⁹ Since lignin is the second major biomass feedstock besides cellulose, but with different chemical structure, an expansion of this approach to lignin would offer new opportunities to produce hybrid bio-inorganic materials with dual functionalities. Although cellulose has a superior mechanical stability than lignin, the latter offers more opportunities for chemical modification due to the unique aromatic structure. However, Bi₄O₅Br₂/BiOBr nanosheets have to be hydrothermally grown under strongly alkaline conditions (pH 13), which makes a direct substitution of the bio-substrate from cellulose to most types of lignin impossible due to dissolution under these conditions.

Fortunately, the chemical properties of lignin depend on the history of pretreatment and the industrially produced hydrolysis lignin is insoluble in strongly alkaline conditions. We were therefore interested to combine photocatalysis and lignin-based sorbents by controlled growth of 2D semiconductors. The industrially produced hydrolysis lignin used in this study was obtained by the percolation hydrolysis.^{20,21} This lignin is an insoluble residue after acid hydrolysis of wood,²² and consists of 48–72% Klason lignin²⁰, while the rest is unreacted cellulose,

mono, and oligosaccharides.²³ Hydrolysis lignin has a very condensed and excessively cross-linked structure, which explains its inability to be dissolved or swelled in any solvents.²⁰ There were several structures of hydrolysis lignin proposed, the one suggested by Chudakov²⁴ is presented in Scheme 1.



Scheme 1. Schematic representation of the structure of hydrolysis lignin.²⁴

Comparing to other lignins, hydrolysis lignin has not found broad application, because of its complicated structure and insolubility without preliminary chemical decomposition.²³ The listed disadvantages are attributed to the impossibility of chemical modification on the molecular level, but could provide advantages for further valorization as a hybrid material. In this work, the key issue was to find a chemically stable biopolymeric material for the deposition of the inorganic photocatalyst in a strong alkali media in an autoclave at 115 °C, and the hydrolysis lignin was found to be excellent and sustainable support for these needs.

We present the successful formation of lignin-inorganic heterojunctions consisting of Bi₄O₅Br₂/BiOBr nanosheets which displays dual functionality. The photoactive lignin-based material can be used simultaneously for removal of i) organic pollutants such as rhodamine B (RhB), methylene blue (MB) dyes, and ii) inorganic pollutants on the examples of cobalt(II), nickel(II) and lead(II) ions. The removal efficiency towards aqueous solutions containing organic dyes and metal ions were studied, including a mechanistic investigation.

EXPERIMENTAL SECTION

Materials. The lignocellulosic material was provided by the company “Santech”. Bi(NO₃)₃·5H₂O, (98%, Alfa Aesar), KBr, (ACS), NaOH, (98–100.5%, Honeywell), NaCl (99.0 %, Acros organics). Ni(NO₃)₂·6H₂O (Puratronic 99.9 wt %) and Co(NO₃)₂·6H₂O (Puratronic 99.9 wt %) were purchased from Alfa Aesar. 4-(2'-Pyridylazo)resorcinol (PAR, 97 %), and Na₂B₄O₇, 98 %, were purchased from Acros organics (Geel, Belgium). Ethanol (≥99.8 %), nitric acid (HNO₃, 65 %), sulphuric acid (H₂SO₄, 95 %), hydrochloric acid (HCl, 37 %), ammonia solution (NH₃ · H₂O, 25 %) were purchased from VWR (Radnor, USA). Rhodamine B dye (RhB), analytical standard, and Methylene Blue dye (MB) were purchased from Sigma. All chemicals were used as received without further purification. All solutions were prepared with deionized water (DI).

Synthesis of Bi₄O₅Br₂/BiOBr. Bi₄O₅Br₂/BiOBr was synthesized according to our previous work¹⁸ Briefly, the hydrothermal treatment of mixture containing Bi(NO₃)₃ and KBr at pH=13 was conducted at 115 °C in a Teflon-lined stainless-steel autoclave.¹⁸

Synthesis of lignin/Bi₄O₅Br₂/BiOBr. 20.6 mM of Bi(NO₃)₃·H₂O and 16.8 mM of KBr were dissolved in 10 mL of DI water and 150 mg of lignin was added. Then, 1 M of NaOH was added dropwise to the mixture to adjust pH 13. The mixture was transferred into a 20 mL Teflon-lined stainless-steel autoclave filled up to 80% of the total volume, after which hydrothermal treatment at 115 °C for 20 h was started. After the reaction, the reactor was allowed cool to room temperature and the precipitate was collected and washed several times with DI water until pH 7.

Structural characterization. FT-IR analysis was performed using a Varian 610-IR FT-IR spectrometer. The samples were analyzed in the range of 600–4000 cm⁻¹ with 16 scans at 4 cm⁻¹ resolution and 1 cm⁻¹ interval at room temperature. Thermal analysis was carried out on a TA Instruments Discovery thermobalance under the next operational conditions: a heating rate of 10 °C·min⁻¹, a dynamic atmosphere of synthetic air of 50 mL·min⁻¹, a temperature range of 30–900 °C, and a sample mass of ~2.5 mg.

The X-ray diffraction (XRD) pattern was determined on a Panalytical X'Pert Alpha1 using Cu Kα (λ = 1.5406 Å) radiation in the 2θ range from 10 to 80°.

Magic-angle-spinning (MAS) NMR experiments were performed at a magnetic field of 14.1 T (Larmor frequencies of 600.12, and 150.92 MHz for ¹H and ¹³C, respectively) on a Bruker Avance-III spectrometer. Spectra were recorded with a 1.3 mm probehead and 60 kHz MAS rate. Proton acquisitions involved a rotor-synchronized, double-adiabatic spin-echo sequence with a 90° excitation pulse of 1.25 μs followed by a pair of 50.0 μs tanh/tanshort high-power adiabatic pulses (SHAPs) with a 5 MHz frequency sweep.^{25,26} All pulses operated at a nutation frequency of 200 kHz. 128 signal transients with a 5 s relaxation delay were collected. The ¹H–¹³C cross-polarization (CP) experiment involved Hartmann–Hahn matched ¹H and ¹³C radiofrequency fields of 20 and 40 kHz, respectively, a 1 ms contact interval for the cross-polarization step, 80 kHz SPINAL-64 ¹H decoupling, and 32768 scans with a 2 s relaxation delay collected. The ¹H and ¹³C chemical shifts were referenced with respect to tetramethylsilane (TMS).

The high-angle annular dark-field (HAADF) images, energy dispersive X-ray spectroscopy (EDX) elemental mappings were collected on a JEOL-2100F in scanning transmission electron microscopy (STEM) mode, and the selected area electron diffraction (SAED) were collected on a JEOL-2100F in Transmission electron microscopy (TEM) mode. Scanning electron microscopy (SEM) and EDX were conducted on a Hitachi field-emission S-4800 microscope with EDX detector (Hitachi, Japan) under the next conditions: an accelerating voltage of 15 kV; emission current of 10.5 μA; the samples were coated with a Pd-Pt layer under a Cressington 208HR high-resolution coater. Carbon tape was used for all samples.

X-ray photoelectron measurement (XPS) was performed in a Prevac photoelectron spectrometer equipped with a hemispherical analyzer (VG SCIENTA R3000). The spectrum was collected using a monochromatized aluminum source AlKα (E = 1486.6 eV) with charge compensation by a low energy electron flood gun (FS40A-PS). The Casa XPS software was applied for the spectrum processing, which included fitting the Shirley background, energy calibration and deconvolution with the mixed function of Gauss and Lorentz (GL = 30).

In order to determine the pH_{PZC}, solutions containing pH values of 2–10 (pH_{initial}) of 0.01 mol·L⁻¹ NaCl in 10 mL flask were prepared using 0.05 mol·L⁻¹ NaOH and 0.05 mol·L⁻¹ HCl. After which, 50 mg of lignin was added to the flask and shaken for 24 h at 180 rpm. The solutions were filtered and the final pH

(pH_e) of the samples were measured using a pH meter and plotted against initial pH. The point of convergence at point zero of the resulting plot (pH_e - pH_{initial}) gives pH_{PZC}.

Photocatalytic Dyes Degradation. 100 ml of 80 mg·L⁻¹ of RhB or MB solutions in DI water were prepared; 0.4 ml of 0.013 M hydrogen peroxide was added. 158 mg of the lignin/Bi₄O₅Br₂/BiOBr composite was added to the solution and this mixture was irradiated with blue light (405 nm, 20 W). 5 mL aliquots from the solution were taken each 20 min up to 100 minutes. The absorption was measured using a Biochrom WPA S800+ Visible Spectrophotometer. The concentration of dyes was calculated from the absorbance values. The photocatalytic tests were conducted in dark in order to avoid any irradiation interference on the sample.

Adsorption and Desorption of RhB and MB. Adsorption tests were performed with the lignin/Bi₄O₅Br₂/BiOBr composite and pristine lignin. In order to perform the adsorption test, 0.4 ml of 0.013 M hydrogen peroxide was added to 100 ml of aqueous solution of RhB or MB with concentration of 80 mg·L⁻¹. 158 mg of the lignin/Bi₄O₅Br₂/BiOBr composite or 150 mg of lignin was then introduced into the solutions. Subsequently, the suspension was shaken in an Orbital Shaker-Incubator ES-20 from Grant-bio at 180 rpm in darkness for 120 minutes. The solution was filtered and allowed to dry. Afterwards, the desorption test was performed on the dried sample. In order to perform desorption, 50 mg of the dried sample was added to 20 mL of ethanol, and shaken for 1 hour. The concentration of the desorbed dye was determined spectrophotometrically using a Biochrom WPA S800+ Visible Spectrophotometer. The desorption percentage (%) was calculated from the ratio of the quantity of adsorbed dye to the quantity of desorbed dye. The desorption percentage was calculated using equation (1).

$$D = \frac{m_{des}}{m_{ads}} \cdot 100 \% \quad (1)$$

where D is the desorption efficiency in percent, m_{des} the amount (mg) of dye in the filtrate after desorption and m_{ads} the initial amount (mg) of dye adsorbed on the sorbent material.

Batch adsorption of Co(II), Ni(II) and Pb(II) ions. Adsorption capacity of lignin was studied using the batch sorption technique. 1 g·L⁻¹ stock solutions of Co(II), Ni(II) and Pb(II) were prepared by dissolving a known amount of Co(NO₃)₂·6H₂O, Ni(NO₃)₂·6H₂O or Pb(NO₃)₂ in DI water. For the adsorption tests, 25 mL of metals solution with known initial ion concentration between 2 mg·L⁻¹ and 160 mg·L⁻¹ at 22 °C were added to the lignin and the suspension shaken in an Orbital Shaker-Incubator ES-20 from Grant-bio at 180 rpm during 2 or 24 hours. The concentration of metal ions was determined by the photometrical methods described by Marchenko et al.²⁷ Absorbance of Co(II) and Pb(II) complexes with 4-(2'-pyridylazo)resorcinol and Ni(II) complexes with dimethylglyoxime were measured at 500 nm, 520 nm and 470 nm, respectively, using an UV-3100PC spectrophotometer (VWR, USA). Samples were measured in triplicates, and average absorbance were applied for further calculations.

The adsorption capacity of the lignin was calculated using the following equation (2):

$$q_{eq} = \frac{(c_0 - c_{eq}) \cdot V}{m_s} \quad (2)$$

where q_{eq} is the amount of metal adsorbed per gram of sorbent (mmol·g⁻¹) at equilibrium, c_0 and c_{eq} are the initial and equilibrium metal ion concentrations (mmol·L⁻¹) in solution, V is the volume (L) of the initial metal ion solution and m_s is the weight of the sorbent (g).

The sorption equilibrium data was applied to the Langmuir, Freundlich and Temkin models. The linear form of the Langmuir model (3):²⁸

$$\frac{c_e}{q_e} = \frac{c_e}{q_0} + \frac{1}{K_L q_0} \quad (3)$$

where q_0 and K_L are adsorption capacity (mmol·g⁻¹) and the Langmuir isotherm constant (L·mmol⁻¹), respectively.

The Freundlich model (4):²⁹

$$\log q_{eq} = \log K_F + \frac{1}{n} \cdot \log c_{eq} \quad (4)$$

where: K_F and n are the Freundlich constants related to the sorption capacity and sorption intensity, respectively.

The Temkin model of isotherm can be expressed as follows (5):

$$q_{eq} = \frac{RT}{b_T} \ln(K_T) + \frac{RT}{b_T} \ln c_{eq} \quad (5)$$

where b_T is the heat of adsorption (kJ·mol⁻¹), K_T is the model constant (L·g⁻¹), R is the gas constant (8.314 J·mol⁻¹·K⁻¹), T represents the absolute temperature (°C).³⁰

RESULTS AND DISCUSSION

Structural characterization of the photoactive lignin/Bi₄O₅Br₂/BiOBr.

Probing the complex and irregular structure of lignin-based materials is a challenging task.^{31,32} Wet chemistry methods such as functional group analysis and degradation techniques provide information in a piecemeal manner, whereas spectroscopic techniques such as IR, Raman, or UV-Vis do not offer sufficient resolution. Among other types of lignin, hydrolysis lignin is even a more challenging material for the characterization due to its insolubility in any solvent. To overcome these limitations, we employed solid-state NMR spectroscopy to gain insight into the structure of hydrolysis lignin directly in the solid-state.³³ In Figure 1, the solid-state ¹H MAS and ¹H-¹³C CPMAS NMR spectra of lignin/Bi₄O₅Br₂/BiOBr are shown. The proton spectrum in panel A reveals signals at 6.6, 3.9, and 1.3 ppm, attributed to aromatic, methoxy (-OCH₃), and aliphatic protons, respectively. Resonances associated with aromatic protons and methoxy groups dominate, and therefore a comparably small amount of aliphatic protons is present in the material. In the ¹H-¹³C CPMAS spectrum presented in panel B, the ¹³C NMR signals is characteristic for different moieties within the lignin structure.³³ The signal at 146 ppm originates from the C-O carbon atom in the aromatic ring, whereas the remaining aromatic carbon atoms contribute to the signals in the chemical shift range of 100–125 ppm (C-H) and 125–135 ppm (C-C). The signals at 89 and 73 ppm correspond to C-α, C-β, and C-γ carbon atoms with -OH groups and those involved in -O-alkyl ethers moieties. Resonances in the 50–65 ppm range can be attributed to methoxy groups, whereas signals ~30 ppm to methyl groups and other saturated aliphatic fragments. The relatively low signal intensity of the ¹³C signal corresponding to methyl groups is in agreement with the proton spectrum. The results of NMR are in good agreement with the proposed highly-condensed structure of hydrolysis lignin (Scheme 1).

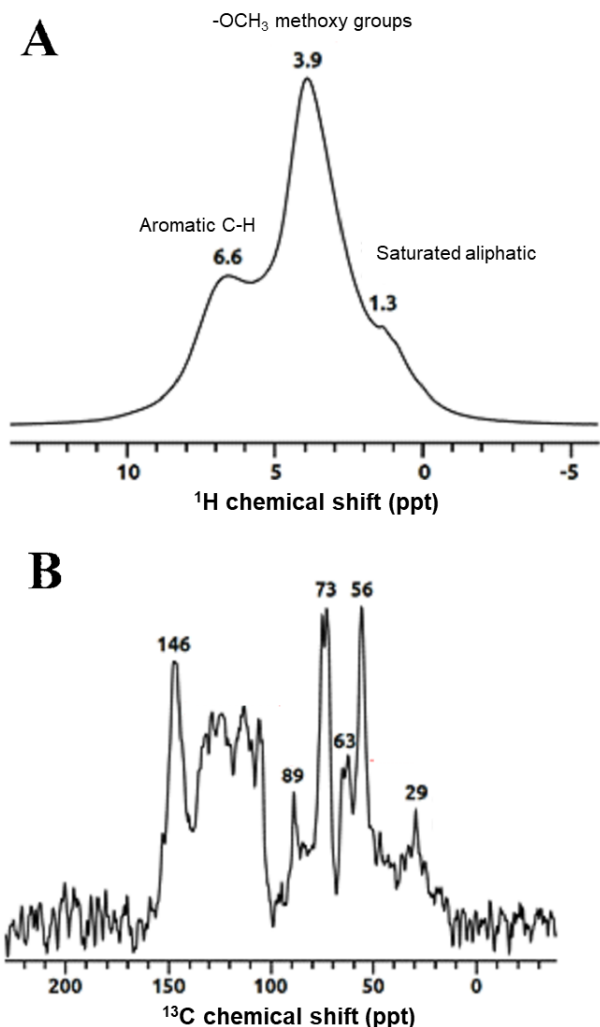


Figure 1. ^1H MAS NMR (A) and ^1H - ^{13}C CPMAS (B) spectra of lignin/ $\text{Bi}_4\text{O}_5\text{Br}_2$ / BiOBr collected at 14.1 T and 60 kHz MAS.

As it was shown in our previous work, two ternary phases $\text{Bi}_4\text{O}_5\text{Br}_2$ and BiOBr could be synthesized as heterojunction nanosheets under relatively mild conditions (115°C). The state of bismuth present on the surface was examined by XPS analysis. In the XPS Bi 4f spectrum (Figure 2A), the spin-orbit split $4f_{7/2}$ and $4f_{5/2}$ features appear. Nevertheless, two different phases containing bismuth can be evidently distinguished. The presence of $\text{Bi}_4\text{O}_5\text{Br}_2$ is manifested by the doublet at 158.4 eV ($4f_{7/2}$) and 163.8 eV ($4f_{5/2}$), whereas BiOBr shows the photoemission at 159.6 eV ($4f_{7/2}$) and 164.9 eV ($4f_{5/2}$).^{34,35} On the other hand, the formation of Bi^{5+} species was not observed as was the case with the previously developed hybrid cellulose-bismuth oxybromide membrane.¹⁸

The fragment of hydrolysis lignin particle with the grown $\text{Bi}_4\text{O}_5\text{Br}_2$ / BiOBr phase is shown on SEM micrograph (Figure 2B) and EDX elements distribution maps (Figure S1). The confirmation of the presence of both phases and its purity was made by employing XRD for the catalyst synthesized without adding lignin (Figure S2). STEM and EDX analysis were conducted as an additional confirmation of presence of $\text{Bi}_4\text{O}_5\text{Br}_2$ and BiOBr phases on the lignin-based support (Figure 3).

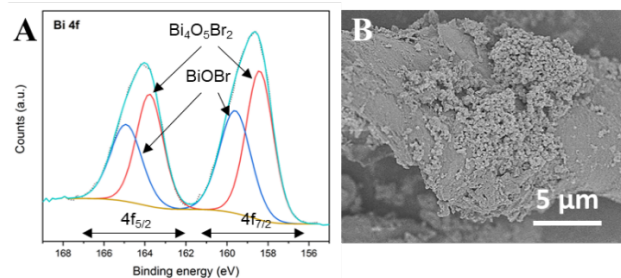


Figure 2. (A) XPS Bi 4f spectrum of the Lignin/ $\text{Bi}_4\text{O}_5\text{Br}_2$ / BiOBr grown on the fragment of hydrolysis lignin showed on (B) SEM micrograph.

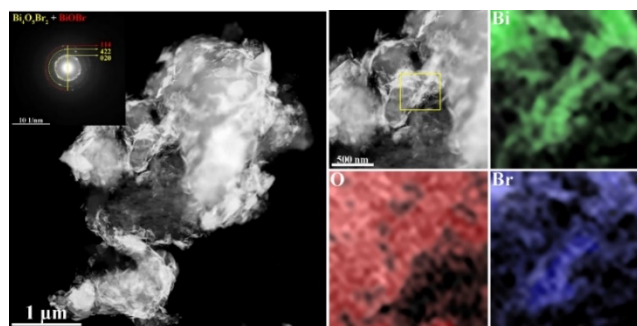


Figure 3. High-angle annular dark-field (HAADF) images and EDX elemental maps.

Since we aimed to develop a material with dual adsorption and photocatalytic functionalities, it was important to preserve the active functional groups of pristine lignin. FTIR spectra were collected for original hydrolysis lignin and hybrid material (Figure S3). The FTIR spectra of both materials are characterized by a broad peak with maximum at 3338 cm^{-1} corresponding to $-\text{OH}$ groups. The spectra show intense bands at 2929 cm^{-1} and 2836 cm^{-1} originating from the presence of CH and methoxy groups, respectively. The comparison of FTIR spectra of initial lignin and the one after the modification has shown that there are no significant changes in the set of characteristic bands and their intensity for both materials (Figure S3), which confirms the preserved original functional groups of lignin.

The content of grown inorganic nanosheets on lignin material was determined using TGA. The comparison of TG-curves of initial lignin and lignin/ $\text{Bi}_4\text{O}_5\text{Br}_2$ / BiOBr has shown that the concentration of $\text{Bi}_4\text{O}_5\text{Br}_2$ / BiOBr in the composite material was 18.9% (Figure S3). Both materials were characterized by $\sim 5\%$ weight loss up to 100°C corresponding to gradual evaporation of moisture.³⁶ High total weight loss (more than 99%) for initial lignin-based material confirmed the absence of impurities such as ash or heavy metals in the sample. The BET surface area was slightly increased from 9.6 to $13.2\text{ m}^2\cdot\text{g}^{-1}$ after lignin modification with the photocatalyst (Figure S5A), which could be caused by increased total pore volume for the composite material ($0.058\text{ cm}^3\cdot\text{g}^{-1}$). From the SEM micrograph of initial lignin material (Figure 4A), the ordered elongated porous nanostructures could be seen, which we attribute to high carbohydrate content in the initial lignin, influencing thus the material structural organization. The lignin/ $\text{Bi}_4\text{O}_5\text{Br}_2$ / BiOBr interface is presented on Figure 4B, where $\text{Bi}_4\text{O}_5\text{Br}_2$ / BiOBr nanosheets are clearly observed (Figure 4B inset).

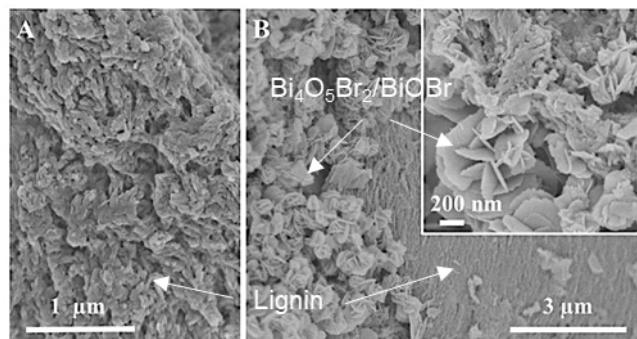


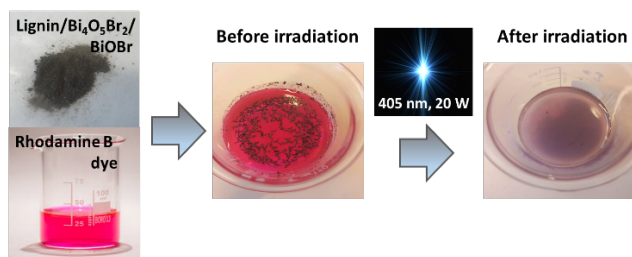
Figure 4. SEM micrographs of (A) initial lignin and (B) Lignin/Bi₄O₅Br₂/BiOBr.

Photodegradation of RhB and MB dye. Since textile wastewaters contain a mixture of anionic and cationic organic dyes, it is important to understand how photodegradation performance is related to the chemical structure of the dye molecule. As such, two dyes were selected for the photodegradation study: zwitterionic RhB and cationic MB dye. Photocatalytic degradation of selected dyes was carried out under illumination of blue light source (405 nm, 20 W). Scheme 2 depicts the applied experimental approach on the example of RhB. It could be seen that after 100 minutes of illumination the solution has a much less intense colour confirming successful elimination of the dye from the solution. The results of RhB and MB dyes photodegradation as a function of time are presented in Figure 5. The photodegradation in presence of the lignin/Bi₄O₅Br₂/BiOBr composite was the most efficient in comparison to other materials tested. The composite lignin material was able to decrease dye concentration from 80 mg·L⁻¹ to 12.3 mg·L⁻¹ for RhB (85% removal) and from 80 mg·L⁻¹ to 4.4 mg·L⁻¹ for MB (95% removal). The Bi₄O₅Br₂/BiOBr interface facilitates charge separation upon illumination due to the type-II heterojunction.^{18,37-39}

In order to examine individually the photocatalytic performance of pure lignin, pure catalyst, and the system without any of those, and also to exclude the influence of adsorption of the dyes by the surface of the composite, the systems were tested separately with the dye solution. It was found that in case of RhB, the pure catalyst or pure lignin have the same performance and eliminate the dye from 80 to 25 mg·L⁻¹ (69%). For the systems with MB, the performance of pure lignin is higher, which could be explained by impact of electrostatic interaction of positively charged MB molecules and negatively charged lignin.⁴⁰ Thus, pure lignin reduced the MB dye concentration from 80 to 25 mg·L⁻¹ (69%), whereas pure catalyst eliminated MB to 51 mg·L⁻¹ (36%). The impact of dyes degradation under the chosen light source without lignin, or without catalyst or lignin/catalyst composite is negligible because of low dye reduction (up to 3% for RhB and up to 5% for MB).

Ethanol is an effective eluent for the desorption of organic dyes from variable materials, e.g. lignin-based materials, because it has a high affinity to organic molecules.⁴¹ The relatively close values of desorption of dyes (up to 10.4% for RhB and up to 3.1% for MB) after adsorption in darkness by pure lignin or lignin/photocatalyst, and lignin/photocatalyst under light irradiation let us assume that this is the percentage of the dye, which was adsorbed by simple diffusion instead of physical adsorption or chemical bonding to the surface of pure lignin or composite material. Both dyes could be binding to lignin-based materials through π -interactions and hydrogen bonds, as well as by electrostatic interactions.⁴¹ Since RhB dye is a zwitterion, the negative charge of MB dye is more dominating and

therefore the electrostatic bonds MB/lignin or lignin/ photocatalyst are stronger.



Scheme 2. Photocatalytic degradation of RhB dye in presence of lignin/Bi₄O₅Br₂/BiOBr.

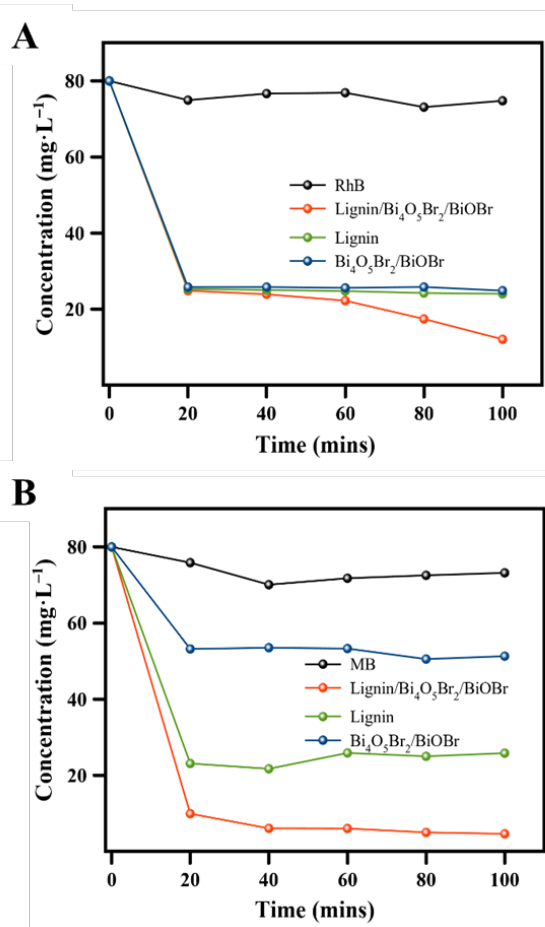


Figure 5. Photocatalytic degradation of (A) RhB and (B) MB in presence of lignin/Bi₄O₅Br₂/BiOBr (Light source 405 nm, 20 W); the loading of the semiconducting photocatalyst (blue curve) was the same as for the lignin/Bi₄O₅Br₂/BiOBr sample: 18.9 mg).

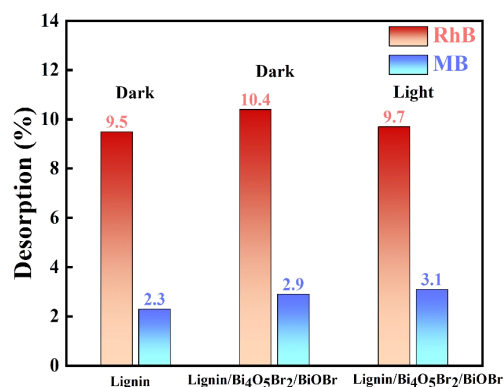


Figure 6. Desorption results of RhB and MB dye, after adsorption pure lignin in darkness, lignin/Bi₄O₅Br₂/BiOBr in darkness and photodegradation of lignin/Bi₄O₅Br₂/BiOBr in light (The samples after contact with dyes solutions were washed with DI water and dried overnight; the desorption by ethanol were conducted afterwards)

The effectiveness of synthesized composite material for both organic and inorganic pollutants is a crucial factor since industrial wastewaters contain broad spectra of contaminants. Therefore, additionally to the study of dyes photodegradation we tested initial lignin and lignin/Bi₄O₅Br₂/BiOBr for the adsorption of cobalt, nickel and lead bivalent ions. According to our previous study,¹⁸ Bi₄O₅Br₂/BiOBr does not have an impact on the adsorption of metal ions, while functionality and structure of biopolymeric support play a major role in the adsorption. Consequently, in this study, we started with an investigation of adsorption efficiency of hydrolysis lignin with respect to bivalent metal ions. Figure 7 depicts adsorption isotherms of Co(II), Ni(II), and Pb(II) ions for the lignin after 2 hours (the same time as needed for the dye degradation) and 24 hours. It was found that all studied metal ions in low initial concentrations have a good affinity to the surface of hydrolysis lignin. With increasing initial concentrations of metal ions, the removal efficiency was decreased greatly for Co(II) and Pb(II) ions. In a selected range of initial concentrations of metal ions, the highest adsorption capacity of lignin was found for Ni(II) ions which reached 0.45 mmol·g⁻¹ after 2 hours and 0.5 mmol·g⁻¹ during 24 hours. It was found that the distribution coefficients for Ni(II) ions were the highest as well: 1.45 and 1.05 L·g⁻¹; for Pb(II) ions: 0.95 and 0.55 L·g⁻¹; and the lowest for Co(II) ions: 0.038 and 0.039 L·g⁻¹ for 2 h and for 24 h, respectively.

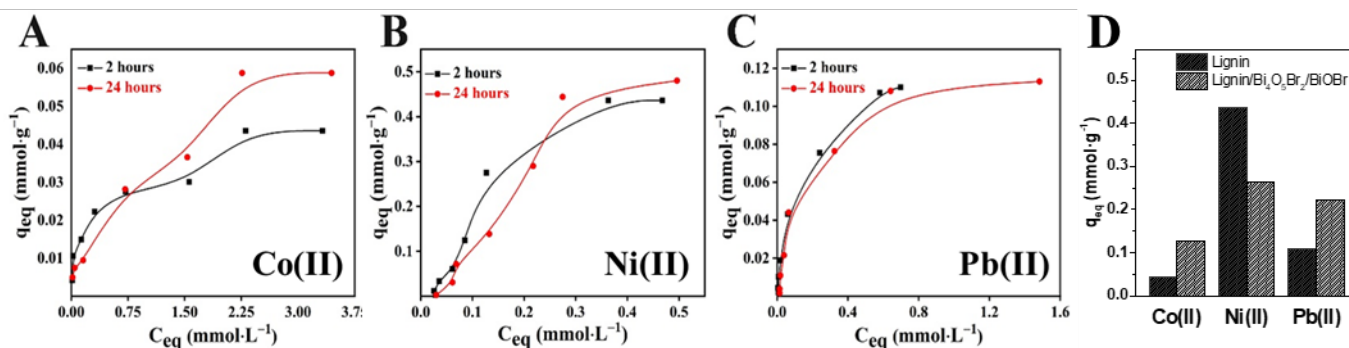


Figure 7. Adsorption isotherms of (A) Co(II), (B) Ni(II) and (C) Pb(II) ions on lignin from aqueous solutions and (D) comparison of adsorption capacity for lignin and lignin/Bi₄O₅Br₂/BiOBr.

Three common isotherm models were applied to describe adsorption of selected metal ions by the surface of hydrolysis lignin. The calculated parameters from the Langmuir, Freundlich and Temkin isotherm models are summarized in Table S1 in SI. The monolayer capacity was found to be up to 0.07 mmol·g⁻¹ for the cobalt(II) ions and up to 0.14 mmol·g⁻¹ for the lead(II) ions. The adsorption was found to be favorable according to the positive values of R_L ($0 < R_L < 1$) for all ions. The heat of adsorption (b_T) was relatively high for all ions: up to 366 kJ·mol⁻¹ for Co(II) ions, up to 16.3 for Ni(II) ions and up to 110 for Pb(II) ions. The lowest values of the maximum binding energy for the interactions between the hydrolysis lignin surface and the Ni(II) ions ($K_T=33.8$ L·g⁻¹ for 2 h, $K_T=20.8$ L·g⁻¹ for 24 h) is in line with the assumption of the highest capacity for used lignin to

Ni(II) ions. The adsorption capacity of pure lignin and the composite towards selected metal ions was compared in Figure 7D. The adsorption capacity towards cobalt and lead aqua complexes increased for the hybrid lignin/Bi₄O₅Br₂/BiOBr composite up to 0.12 and 0.22 mmol·g⁻¹ during 2 h phase contact. For Ni(II) ions, the capacity was higher for initial lignin (0.45 mmol·g⁻¹) compared to the composite (0.26 mmol·g⁻¹). The pH_{pzc} for the composite is 8.5, which indicates that in neutral media the composite is positively charged (Figure S6). This highlights that lignin/Bi₄O₅Br₂/BiOBr is a promising material with complimentary photocatalytic and adsorption properties towards synthetic dyes and metal ions.

CONCLUSION

We presented the *LignoPhot* concept which offers the opportunity to hydrothermally prepare bio-inorganic hybrid composites from lignin and photocatalysts from the ternary Bi-O-Br system. The unique advantage is the combination of photocatalytic activity towards organic dyes (with variable charge) and adsorption of metal ions. Both types of compounds are usually simultaneously present in industrial wastewaters. The hydrolysis lignin structure and functionality was investigated by means

of ¹H-¹³C CPMAS NMR, which confirmed its highly-condensed structure. The state of bismuth present on the lignin surface was determined by XPS analysis. From SEM micrographs it was found that the Bi₄O₅Br₂/BiOBr nanosheets interface were grown on the lignin surface, where HAADF and EDX confirmed the homogeneous distribution of the inorganic phase on lignin support. Lignin/Bi₄O₅Br₂/BiOBr was shown prominent photocatalytic activity towards RhB and MB dyes oxidation under irradiation at 405 nm (20W). With respect to the complementary adsorption function, the composite lignin material was

able to decrease the dye concentration from 80 mg·L⁻¹ to 12.3 mg·L⁻¹ for RhD (85%) and from 80 mg·L⁻¹ to 4.4 mg·L⁻¹ for MB (95%), which is much higher than for the systems with dye/lignin, dye/catalyst or just dye. As an additional advantage of the material, the composite exhibits a high performance as a sorbent for metal ions. The corresponding adsorption capacity towards Co(II), Ni(II) and Pb(II) was 0.12, 0.26 and 0.22 mmol·g⁻¹, respectively. The investigation on adsorption of selected metal ions on the lignin support showed that Co(II), Ni(II) and Pb(II) ions in low initial concentrations have a good affinity to the surface of hydrolysis lignin, which is in good agreement with the determined distribution coefficients: 1.45 and 1.05 L·g⁻¹ for Ni(II) ions; 0.95 and 0.55 L·g⁻¹ for Pb(II) ions; 0.038 and 0.039 L·g⁻¹ for Co(II) ions for 2 h and for 24 h, respectively. In a selected range of initial concentrations of metal ions, the highest adsorption capacity of initial lignin was found for Ni(II) ions, which reached 0.45 mmol·g⁻¹ after 2 hours of phase contact (the distribution coefficient for Ni(II) ions was 1.45 L·g⁻¹). Our study unravels the opportunities of lignin as a substrate to achieve a controlled growth of semiconductor nanostructures on its surface while maintaining the functional groups of the biopolymer.

ASSOCIATED CONTENT

Supporting Information.

The Supporting Information is available free of charge on the ACS Publications website at DOI: XRD patterns; FTIR spectra; thermal analysis; N₂ adsorption/desorption isotherms; isotherm model parameters obtained for Co(II), Ni(II) and Pb(II) ions adsorption onto hydrolysis lignin.

AUTHOR INFORMATION

Corresponding Authors

Adam Slabon - Department of Materials and Environmental Chemistry, Stockholm University, Svante Arrhenius väg 16 C, 106 91 Stockholm, Sweden; ORCID: 0000-0002-4452-1831
Email: adam.slabon@mmk.su.se

Authors

Tetyana M. Budnyak – Department of Materials and Environmental Chemistry, Stockholm University, Svante Arrhenius väg 16C, 106 91 Stockholm, Sweden; ORCID: 0000-0003-2112-9308

Joy Onwumere – Department of Materials and Environmental Chemistry, Stockholm University, Svante Arrhenius väg 16C, 106 91 Stockholm, Sweden; AC2T research GmbH, 2700 Wiener Neustadt, Austria; ORCID: 0000-0002-6889-0527;

Ievgen V. Pylypchuk – Department of Fiber and Polymer Technology, KTH Royal Institute of Technology, Teknikringen 56-58, SE-100 44 Stockholm, Sweden; ORCID: 0000-0001-5467-2839

Aleksander Jaworski – Department of Materials and Environmental Chemistry, Stockholm University, Svante Arrhenius väg 16C, 106 91 Stockholm, Sweden; ORCID: 0000-0002-7156-559X

Jianhong Chen – Department of Materials and Environmental Chemistry, Stockholm University, Svante Arrhenius väg 16C, 106 91 Stockholm, Sweden; ORCID: 0000-0001-9020-1786

Anna Rokicińska – Faculty of Chemistry, Jagiellonian University, Gronostajowa 2, 30-387 Kraków, Poland; ORCID: 0000-0001-8397-4422

Olena Sevastyanova – Department of Fiber and Polymer Technology, Wallenberg Wood Science Center (WWSC), KTH Royal Institute of Technology, Teknikringen 56-58, SE-100 44 Stockholm, Sweden; ORCID: 0000-0001-7433-0350

Mikael E. Lindström – Department of Fiber and Polymer Technology, KTH Royal Institute of Technology, Teknikringen 56-58, SE-100 44 Stockholm, Sweden; ORCID: 0000-0002-2900-4713

Piotr Kuśtrowski – Faculty of Chemistry, Jagiellonian University, Gronostajowa 2, 30-387 Kraków, Poland; ORCID: 0000-0001-8496-0559

Author Contributions

§ These authors contributed equally. All authors have approved the final version of the manuscript.

ACKNOWLEDGMENT

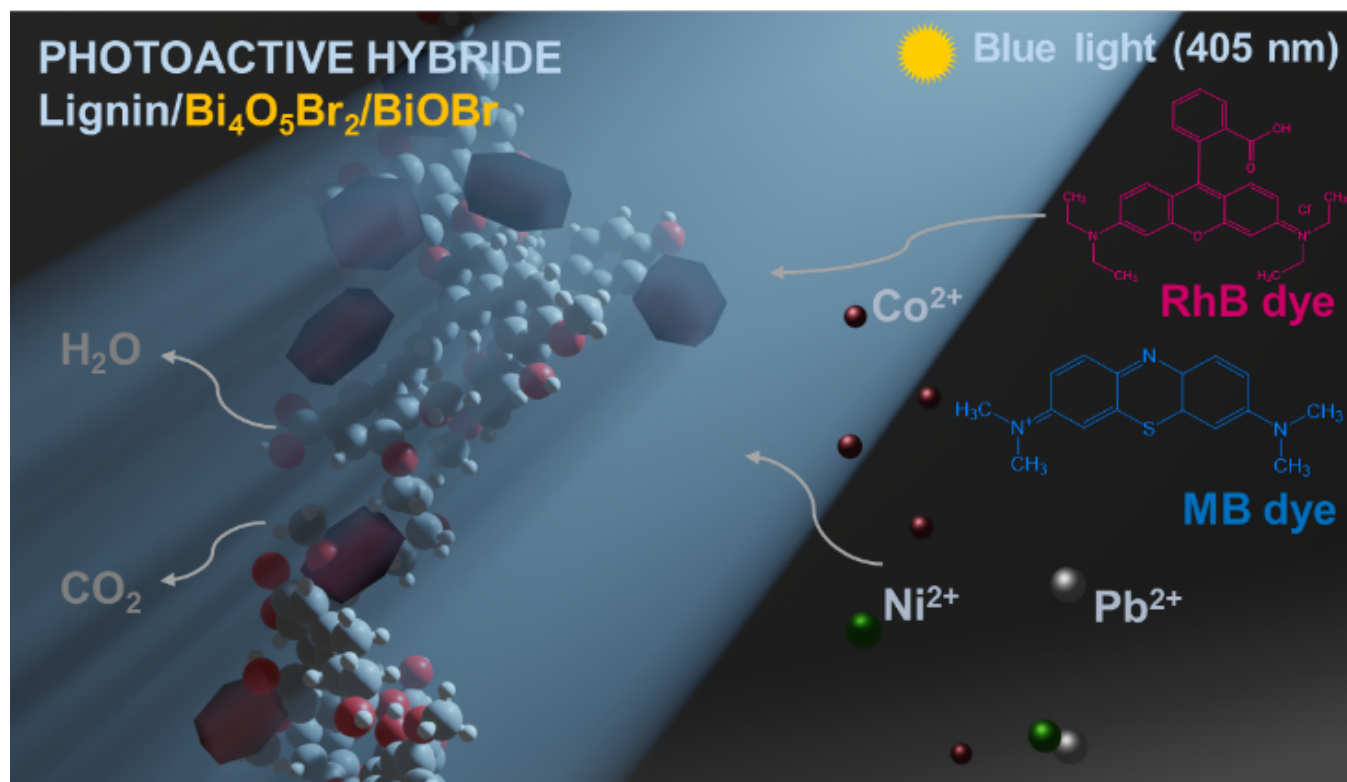
This project was financially supported by Swedish Foundation for Strategic Environmental Research (project: Mistra SafeChem, project number 2018/11). T.M.B. acknowledges financial support from the ÅForsk Foundation (grant number 19-676). Ie.P. acknowledges the Wood and Pulping Chemistry Research Network (WPCRN) for the financial support of his work. P.K. acknowledges the European Regional Development Fund in the framework of the Polish Innovation Operational Program (contract no. POIG.02.01.00-12-023/08) for financial support.

REFERENCES

- (1) Government offices of Sweden. Press release from Ministry of Enterprise and Innovation, Ministry of the Environment “Sweden transitioning to a circular economy.”
- (2) Mani, S.; Bharagava, R. N. Textile Industry Wastewater Environmental and Health Hazards and Treatment Approaches. In *Recent Advances in Environmental Management*; CRC Press, 2018; Vol. 1, pp 47–69.
- (3) Yaseen, D. A.; Scholz, M. *Textile Dye Wastewater Characteristics and Constituents of Synthetic Effluents: A Critical Review*; Springer Berlin Heidelberg, 2019; Vol. 16. <https://doi.org/10.1007/s13762-018-2130-z>.
- (4) Singh R.P.; P.K., S.; R., G.; R.L., S. Treatment and Recycling of Wastewater from Textile Industry. In *Advances in Biological Treatment of Industrial Waste Water and their Recycling for a Sustainable Future. Applied Environmental Science and Engineering for a Sustainable Future*; Singh, R., Singh, R., Eds.; Springer: Singapore, 2019. https://doi.org/https://doi.org/10.1007/978-981-13-1468-1_8.
- (5) Szewczyk, I.; Rokicińska, A.; Michalik, M.; Chen, J.; Jaworski, A.; Aleksis, R.; Pell, A. J.; Hedin, N.; Slabon, A.; Kuśtrowski, P. Electrochemical Denitrification and Oxidative Dehydrogenation of Ethylbenzene over N-Doped Mesoporous Carbon: Atomic Level Understanding of Catalytic Activity by 15 N NMR Spectroscopy. *Chem. Mater.* **2020**, *32* (17), 7263–7273. <https://doi.org/10.1021/acs.chemmater.0c01666>.
- (6) Deng, J.; Su, Y.; Liu, D.; Yang, P.; Liu, B.; Liu, C. Nanowire Photoelectrochemistry. *Chem. Rev.* **2019**, *119* (15), 9221–9259. <https://doi.org/10.1021/acs.chemrev.9b00232>.
- (7) Chen, Z.; Löber, M.; Rokicińska, A.; Ma, Z.; Chen, J.; Kuśtrowski, P.; Meyer, H. J.; Dronskowski, R.; Slabon, A. Increased Photocurrent of CuWO₄ Photoanodes by Modification with the Oxide Carbodiimide Sn₂O(NCN). *Dalt. Trans.* **2020**, *49* (11), 3450–3456. <https://doi.org/10.1039/c9dt04752b>.
- (8) Cho, J.; Suwandaratne, N. S.; Razeq, S.; Choi, Y. H.; Piper, L. F. J.; Watson, D. F.; Banerjee, S. Elucidating the Mechanistic Origins of Photocatalytic Hydrogen Evolution Mediated by MoS₂/CdS Quantum-Dot Heterostructures. *ACS Appl. Mater. Interfaces* **2020**, *12* (39), 43728–43740. <https://doi.org/10.1021/acsami.0c12583>.
- (9) Kato, D.; Hongo, K.; Maezono, R.; Higashi, M.; Kunioku, H.; Yabuuchi, M.; Suzuki, H.; Okajima, H.; Zhong, C.; Nakano, K.; Abe, R.; Kageyama, H. Valence Band Engineering of Layered Bismuth Oxyhalides toward Stable Visible-Light Water Splitting: Madelung Site Potential Analysis. *J. Am. Chem. Soc.* **2017**, *139*

- (51), 18725–18731. <https://doi.org/10.1021/jacs.7b11497>.
- (10) Kageyama, H.; Hayashi, K.; Maeda, K.; Atfield, J. P.; Hiroi, Z.; Rondinelli, J. M.; Poepelmeier, K. R. Expanding Frontiers in Materials Chemistry and Physics with Multiple Anions. *Nat. Commun.* **2018**, *9* (1). <https://doi.org/10.1038/s41467-018-02838-4>.
- (11) Ji, M.; Di, J.; Ge, Y.; Xia, J.; Li, H. 2D-2D Stacking of Graphene-like g-C 3 N 4 /Ultrathin Bi 4 O 5 Br 2 with Matched Energy Band Structure towards Antibiotic Removal. *Appl. Surf. Sci.* **2017**, *413*, 372–380. <https://doi.org/10.1016/j.apsusc.2017.03.287>.
- (12) Schilling, W.; Das, S. CO₂-Catalyzed/Promoted Transformation of Organic Functional Groups. *Tetrahedron Lett.* **2018**, *59* (43), 3821–3828. <https://doi.org/https://doi.org/10.1016/j.tetlet.2018.08.033>.
- (13) Riemer, D.; Schilling, W.; Goetz, A.; Zhang, Y.; Gehrke, S.; Tkach, I.; Hollóczki, O.; Das, S. CO₂-Catalyzed Efficient Dehydrogenation of Amines with Detailed Mechanistic and Kinetic Studies. *ACS Catal.* **2018**, *8* (12), 11679–11687. <https://doi.org/10.1021/acscatal.8b03059>.
- (14) Zhang, Y.; Zhang, T.; Das, S. Catalytic Transformation of CO₂ into C1 Chemicals Using Hydrosilanes as a Reducing Agent. *Green Chem.* **2020**, *22* (6), 1800–1820. <https://doi.org/10.1039/C9GC04342J>.
- (15) Wang, Z. Green Chemistry: Recent Advances in Developing Catalytic Processes in Environmentally-Benign Solvent Systems. *Front. Chem.* **2008**, 1–43.
- (16) Anastas, P. T.; Zimmerman, J. B. Design through the 12 Principles of Green Engineering. *IEEE Eng. Manag. Rev.* **2007**, *35* (3), 16. <https://doi.org/10.1109/EMR.2007.4296421>.
- (17) Moreno, A.; Sipponen, M. H. Lignin-Based Smart Materials: A Roadmap to Processing and Synthesis for Current and Future Applications. *Mater. Horizons* **2020**, *7* (9), 2237–2257. <https://doi.org/10.1039/d0mh00798f>.
- (18) Onwumere, J.; Piątek, J.; Budnyak, T.; Chen, J.; Budnyk, S.; Karim, Z.; Thersleff, T.; Kuśtrowski, P.; Mathew, A. P.; Slabon, A. CelluPhot: Hybrid Cellulose– Bismuth Oxybromide Membrane for Pollutant Removal. *ACS Appl. Mater. Interfaces* **2020**, *12* (38), 42891–42901.
- (19) Nair, S. S.; Chen, J.; Slabon, A.; Mathew, A. P. Converting Cellulose Nanocrystals into Photocatalysts by Functionalisation with Titanium Dioxide Nanorods and Gold Nanocrystals. *RSC Adv.* **2020**, *10* (61), 37374–37381. <https://doi.org/10.1039/d0ra05961g>.
- (20) Rabinovich, M. L.; Fedoryak, O.; Dobeles, G.; Andersone, A.; Gawdzik, B.; Lindström, M. E.; Sevastyanova, O. Carbon Adsorbents from Industrial Hydrolysis Lignin: The USSR/Eastern European Experience and Its Importance for Modern Biorefineries. *Renew. Sustain. Energy Rev.* **2016**, *57*, 1008–1024. <https://doi.org/10.1016/j.rser.2015.12.206>.
- (21) Yuan, Z.; Browne, C. T.; Zhang, X. Biomass Fractionation Process for Bioproducts, World Patent, WO2011057413A1, 2012. Retrieved Novemb. **2014**.
- (22) Chen, H. *Lignocellulose Biorefinery Feedstock Engineering*; 2015. <https://doi.org/10.1016/b978-0-08-100135-6.00003-x>.
- (23) Mahmood, N.; Yuan, Z.; Schmidt, J.; Xu, C. (Charles). Hydrolytic Depolymerization of Hydrolysis Lignin: Effects of Catalysts and Solvents. *Bioresour. Technol.* **2015**, *190*, 416–419. <https://doi.org/https://doi.org/10.1016/j.biortech.2015.04.074>.
- (24) Chudakov, M. I. Industrial Use of Lignin. *Lesn. Promyshlennost', Moscow* **1983**.
- (25) Kervern, G.; Pintacuda, G.; Emsley, L. Fast Adiabatic Pulses for Solid-State NMR of Paramagnetic Systems. *Chem. Phys. Lett.* **2007**, *435* (1–3), 157–162. <https://doi.org/10.1016/j.cplett.2006.12.056>.
- (26) Hwang, T. L.; Van Zijl, P. C. M.; Garwood, M. Fast Broadband Inversion by Adiabatic Pulses. *Journal of Magnetic Resonance*. 1998. <https://doi.org/10.1006/jmre.1998.1441>.
- (27) M. Marchenko. Photometric Detection of Traces of Elements. **1971**.
- (28) Langmuir, I. The Constitution and Fundamental Properties of Solids and Liquids. Part I. Solids. *J. Am. Chem. Soc.* **1916**, *38* (11), 2221–2295.
- (29) Freundlich, H. Über Die Adsorption in Lösungen. *Zeitschrift für Phys. Chemie* **2017**, *57U* (1). <https://doi.org/10.1515/zpch-1907-5723>.
- (30) Foo, K. Y.; Hameed, B. H. Insights into the Modeling of Adsorption Isotherm Systems. *Chem. Eng. J.* **2010**, *156* (1), 2–10. <https://doi.org/10.1016/j.cej.2009.09.013>.
- (31) Pylypchuk, I. V.; Lindén, P. A.; Lindström, M. E.; Sevastyanova, O. New Insight into the Surface Structure of Lignin Nanoparticles Revealed by 1H Liquid-State NMR Spectroscopy. *ACS Sustain. Chem. Eng.* **2020**, *8* (36), 13805–13812. <https://doi.org/10.1021/acssuschemeng.0c05119>.
- (32) Giummarella, N.; Pylypchuk, I. V.; Sevastyanova, O.; Lawoko, M. New Structures in Eucalyptus Kraft Lignin with Complex Mechanistic Implications. *ACS Sustain. Chem. Eng.* **2020**, *8* (29), 10983–10994. <https://doi.org/10.1021/acssuschemeng.0c03776>.
- (33) Capanema, E. A.; Balakshin, M. Y.; Kadla, J. F. A Comprehensive Approach for Quantitative Lignin Characterization by NMR Spectroscopy. *J. Agric. Food Chem.* **2004**, *52* (7), 1850–1860.
- (34) Li, R.; Xie, F.; Liu, J.; Wang, Y.; Wang, Y.; Zhang, X.; Fan, C. Synthesis of Bi₄O₅Br₂ from Reorganization of BiOBr and Its Excellent Visible Light Photocatalytic Activity. *Dalt. Trans.* **2016**, *45* (22), 9182–9186. <https://doi.org/10.1039/c6dt00997b>.
- (35) Di, J.; Xia, J.; Ji, M.; Yin, S.; Li, H.; Xu, H.; Zhang, Q.; Li, H. Controllable Synthesis of Bi₄O₅Br₂ Ultrathin Nanosheets for Photocatalytic Removal of Ciprofloxacin and Mechanism Insight. *J. Mater. Chem. A* **2015**, *3* (29), 15108–15118. <https://doi.org/10.1039/c5ta02388b>.
- (36) Budnyak, T. M.; Aminzadeh, S.; Pylypchuk, I. V.; Riazanova, A. V.; Tertykh, V. A.; Lindström, M. E.; Sevastyanova, O. Peculiarities of Synthesis and Properties of Lignin–Silica Nanocomposites Prepared by Sol–Gel Method. *Nanomaterials* **2018**, *8* (11), 950–967.
- (37) Lu, C.; Ma, Z.; Jäger, J.; Budnyak, T. M.; Dronskowski, R.; Rokicińska, A.; Kuśtrowski, P.; Pammer, F.; Slabon, A. NiO/Poly(4-Alkylthiazole) Hybrid Interface for Promoting Spatial Charge Separation in Photoelectrochemical Water Reduction. *ACS Appl. Mater. Interfaces* **2020**, *12* (26), 29173–29180. <https://doi.org/10.1021/acsami.0c03975>.
- (38) Liu, D.; Yao, W.; Wang, J.; Liu, Y.; Zhang, M.; Zhu, Y. Enhanced Visible Light Photocatalytic Performance of a Novel Heterostructured Bi₄O₅Br₂/Bi₂O₃1Br/10Bi₂SiO₅ Photocatalyst. *Appl. Catal. B Environ.* **2015**, *172–173*, 100–107. <https://doi.org/10.1016/j.apcatb.2015.01.037>.
- (39) Lu, C.; Driichel, A.; Chen, J.; Enders, F.; Rokici, A.; Dronskowski, R.; Boldt, K.; Slabon, A. Nanoscale ZnSe Quantum Dots for Photoelectrochemical Water Reduction †. *Nanoscale*. <https://doi.org/10.1039/d0nr06993k>.
- (40) Budnyak, T. M.; Aminzadeh, S.; Pylypchuk, I. V.; Sternik, D.; Tertykh, V. A.; Lindström, M. E.; Sevastyanova, O. Journal of Environmental Chemical Engineering Methylene Blue Dye Sorption by Hybrid Materials from Technical Lignins. *J. Environ. Chem. Eng.* **2018**, *6* (4), 4997–5007. <https://doi.org/10.1016/j.jece.2018.07.041>.
- (41) Budnyak, T. M.; Aminzadeh, S.; Pylypchuk, I. V.; Sternik, D.; Tertykh, V. A.; Lindström, M. E.; Sevastyanova, O. Methylene Blue Dye Sorption by Hybrid Materials from Technical Lignins. *J. Environ. Chem. Eng.* **2018**, *6* (4), 4997–5007. <https://doi.org/10.1016/j.jece.2018.07.041>.

TOC



Synopsis:

Hybrid lignin/Bi₄O₅Br₂/BiOBr composite with dual functionality for wastewater purification.